A Theoretical Model for Separation in the Fluid Jet Amplifier

Abstract: A theoretical study, based on the re-entrant jet model, is made of the growth of the separation region in the fluid jet amplifier. The flow is taken to be inviscid but dissipation of momentum is obtained by means of the re-entrant jet. The effect of control port pressure and wall angle on the size of the separation region is calculated. Several other versions of the model are suggested.

Nomenclature

Physical quantities

 α ratio between the uniform jet velocity far upstream and that along the free boundary of the re-entrant jet

 β angle between the wall and the axis of the channel (see Fig. 4a)

d offset of the wall (see Fig. 4a)

 s_D location of the stagnation point (see Fig. 4a)

 δ_C , δ_F downstream widths of the main jet and the reentrant jet, respectively, normalized with respect to the upstream jet width

Mathematical symbols

z = x + iy	complex coordinates in the physical
	plane
$\zeta = u - iv = qe^{-i\theta}$	complex velocity
w	complex potential
$\Omega = -\ln \zeta$	see Eq. (1)
t	auxiliary complex plane
t_A, t_D, t_E	points on the t-plane corresponding
	to A , D , E on the Ω - and w -plane
k, k', ψ_2	defined in Eqs. (18) and (19)
K, E; K', E'	complete elliptic integrals of the
	first and second kind of moduli k
	and k' , respectively
$F(\psi_2, k'), E(\psi_2, k')$	incomplete elliptic integrals of the
	first and second kind of argument

 ψ_2 and modulus k', respectively

1. Introduction

The fluid jet amplifier is a bistable device that offers possibilities as a logic element for computers and as a control element. It operates by switching the direction of flow of a jet and depends on flow separation, jet entrainment, and reattachment for its nonlinear characteristics. In the past few years, since the announcement of the development of the device¹, considerable experimental work has been done.²⁻⁴ Little theoretical analysis has been published thus far, but this is not surprising since the problems of boundary layer separation, jet reattachment, and turbulent jet entrainment have long presented analytical difficulties. In this paper one aspect of the flow is considered. A hydrodynamic model is introduced for the particular flow separation that seems important in the operation of a jet amplifier.

There have been, of course, a number of treatments of flow separation and of jet entrainment and reattachment. The applications of Coanda⁵ depend on a recognition of these properties of bounded jet flows. Recently, Bourque and Newman⁶, Newman⁷, and others⁸ have discussed aspects of the problem. In particular, Newman has considered a geometry quite close to that of the jet amplifier.⁷ He has, in fact, taken a constant-pressure region as a part of the separation model just as we do. As can be seen, however, in the sketch of the device shown in Fig. 1, as the jet issues from the channel it is subjected to controlling pressures and flows from the right- and left-hand control ports. These produce the switching of the jet from one wall to the other, which is the desired operation.

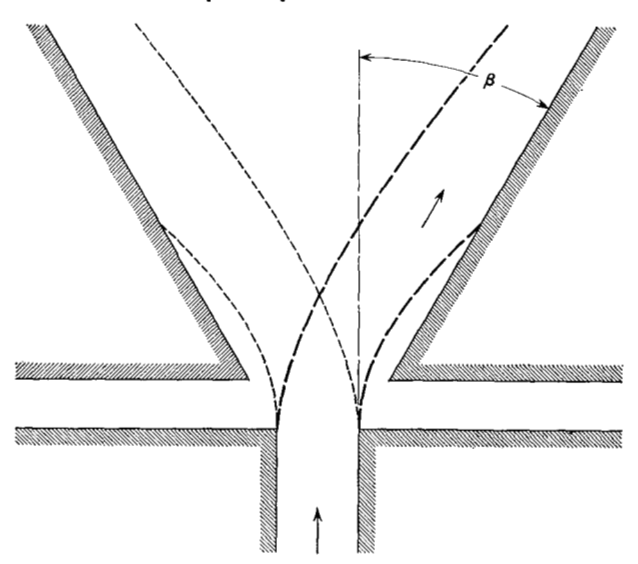
This imposing of conditions in control regions on the boundaries of the jet brings in an element which is not usually present in jet attachment considerations. In the problem discussed by Newman, for instance, the separation region is formed between the jet boundary and the solid wall, and the pressure inside the region is not to be imposed but rather to be determined as a function of the geometry and the flow parameters of the jet. In the jet amplifier the pressure and flow in this region are imposed.

Our model must therefore allow the pressure in this region to be an independent variable of the flow. Furthermore, it is desirable that calculations can be made for any value of the angle β . The model used by Newman⁷ is not valid for small angles. It should be pointed out that the applications in mind here call for this flow to take place in channels which are deep enough so that a two-dimensional analysis is appropriate.

Since it is quite clear that viscous effects play an important role in the separation and in the other fluid phenomena, it may seem strange to choose an inviscid fluid model, as is done in this analysis. The use of the reentrant jet model which is adopted here does, however, allow for momentum dissipation. In a way this is just what is accomplished in other calculations which use empirical or semi-empirical notions of turbulent jet entrainment.

A series of flow models can be constructed of varying degrees of complexity and, correspondingly, of different degrees of mathematical difficulty. Such a series is shown in Figs. 2, 3, and 4. The detailed analysis in the present paper has been carried out for the flow in Fig. 4 since it is the simplest of the three. As will be evident, however, it is not so simple to calculate even for this case. It seems worthwhile, however, to describe the other two models.

Figure 1 Fluid jet amplifier.

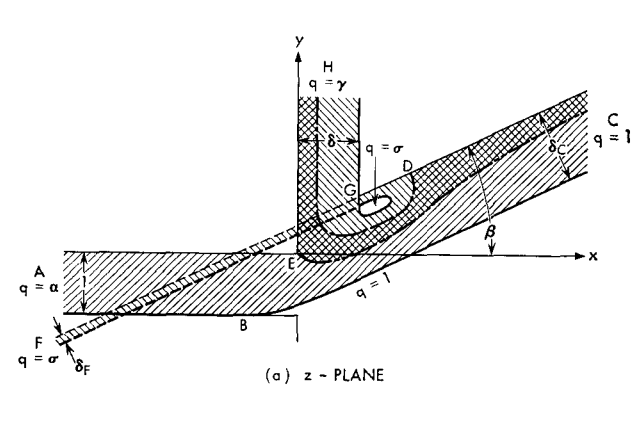


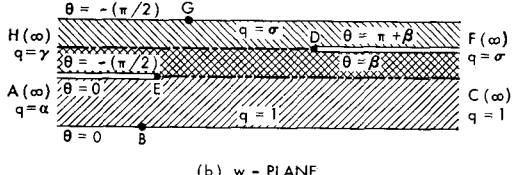
In Figs. 2 and 3 the fluid issues from a channel at E and B. In Fig. 2 there is a streamline from E to C which separates this main jet flow from the fluid from the control port at E and G. This control flow is divided into two portions, one of which goes downstream toward C, joining the main jet flow. The other part curves around a constant-pressure region and flows back into a re-entrant jet. The streamline which detaches from G is one along which the pressure and, therefore, for this time-independent flow, the velocity is constant. The re-entering jet is assumed to go off onto a second Riemann sheet in the physical plane in the same manner as the re-entrant jet of cavitation flow theory created by Efros⁹ and Kreisel.¹⁰ In Fig. 2, D is a stagnation point; the flow from DF is assumed to have the angle of the wall GC. It is to be understood that G lies below the jet, not on the same sheet as F.

It is well known that a flow with a constant pressure region of finite length cannot exist within exact, incompressible, nonviscous potential theory. It is necessary to introduce an artifice such as the re-entrant jet in order that the physically expected properties, such as drag or momentum loss and the correct boundary curvatures, can be accounted for. In doing so, one can also consider that the momentum removed is a kind of dissipation, modeled by potential processes. This is really at the heart of all potential wake theories that originate from the ideas of Kirchhoff and Helmholtz. On the other hand, the re-entrant jet destroys fluid, but one may think of this fluid as becoming the secondary, circulating flow of the separation region. If the amount of fluid removed to the second Riemann sheet is small, this seems to be a reasonable idea. The size of the separation region is to be measured in terms of the position of the stagnation point D.

Another version of this flow is shown in Fig. 3. This is a simpler case in that all of the control flow forms the reentrant jet; it is all dissipated. In Fig. 4 an even simpler case is shown in which the control port allows no fluid to enter but presents only a constant pressure to the main jet. The secondary flow and the separation region is formed by fluid from the main jet. There is a streamline AD which separates the fluid going downstream and that going into the re-entrant jet. The free streamline detaches at E and forms with AD the boundaries of the re-entrant jet. In this case, instead of a channel flow, the main stream is a jet along the solid wall AE with the free boundary extending from A to C.

These flows all have much in common with the reentrant jet cavity flow at the nose of a wedge at angle of attack, a problem discussed by Cox and Clayden.¹¹ They are actually somewhat simpler in that, as will be seen, they are not doubly covered in the complex velocity plane as is the case in Ref. 11.





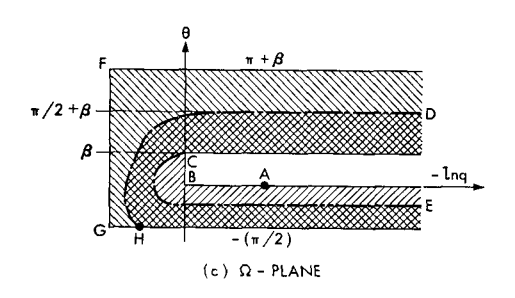
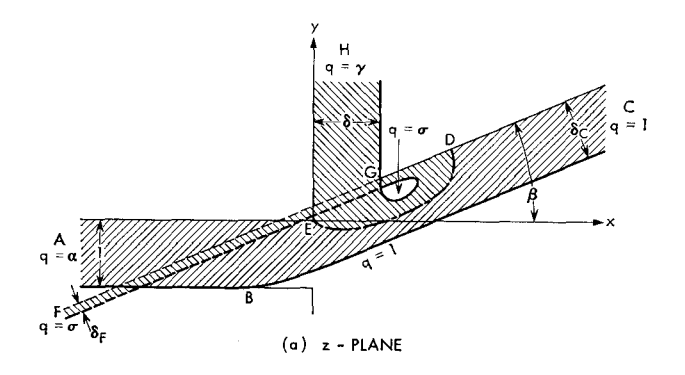
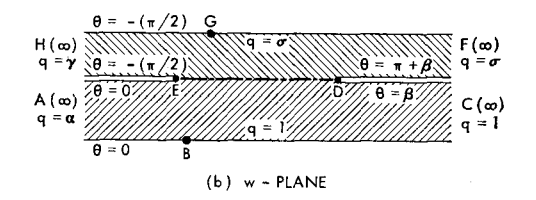


Figure 2 Jet flow pattern with control port flow (I).





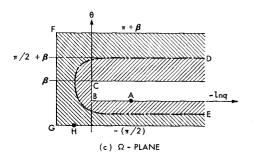


Figure 3 Jet flow pattern with control port flow (II).

The three cases exhibited form a hierarchy of models of reducing order of complexity. This can be well understood by looking at Figs. 2b,c, 3b,c, and 4b,c. If one takes the velocity of the flow to be in complex form $\zeta = u - iv = qe^{-i\theta}$ and the complex potential to be w(z), z = x + iy, then $dw/dz = \zeta$. It is useful to define

$$\Omega = -\ln \zeta = -\ln q + i\theta. \tag{1}$$

Then

$$\zeta = e^{-n}$$

and

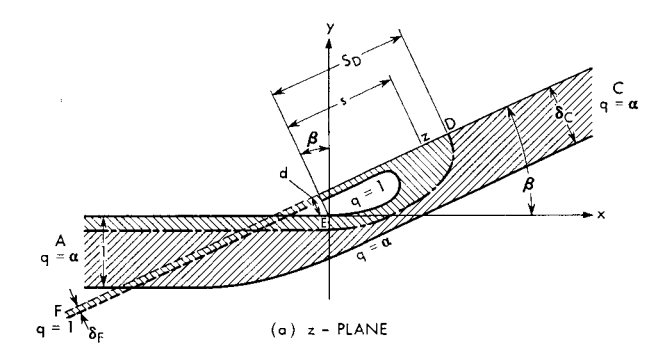
$$z = \int \frac{1}{\zeta} dw = \int e^{\Omega} dw.$$
 (2)

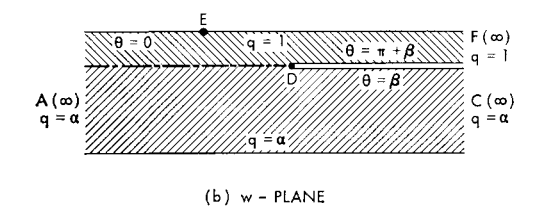
Following the classical hodograph methods of solving free streamline flows, the w- plane and the Ω -plane are to be mapped simultaneously onto an auxiliary half-plane, t. In Figs. 2, 3, and 4 the w- and Ω -planes are shown for each case. The increasing simplicity becomes quite clear

although the procedure will remain quite the same.

The calculation which follows uses the model of Fig. 4 as a first effort in understanding the usefulness of the reentrant jet model in this context. As will be seen, the analytical expressions produced for the separation region size, s_D , as a function of the other flow parameters are quite complex and require numerical handling.

In Section 2 of the paper the details of the analysis are set out. In Section 3 there is an explanation of the numerical analysis and in Section 4 a discussion of the calculated results. The location of the reattachment point in this theory is a function of the control port pressure and the angle β . The theory seems to fit into the results obtained by Newman⁷, whose calculations were carried out for larger angles than were considered in ours. Small angles, less than 20°, are the appropriate range for the jet amplifier. There is no reason, however, why large-angle calculations cannot be made from our flow model whereas Newman's theory is restricted to small angles. The reattachment values obtained here depend on two variables





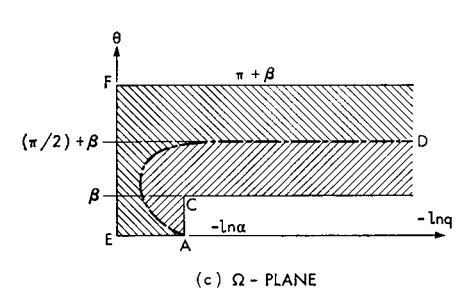


Figure 4 Jet flow pattern without control port flow.

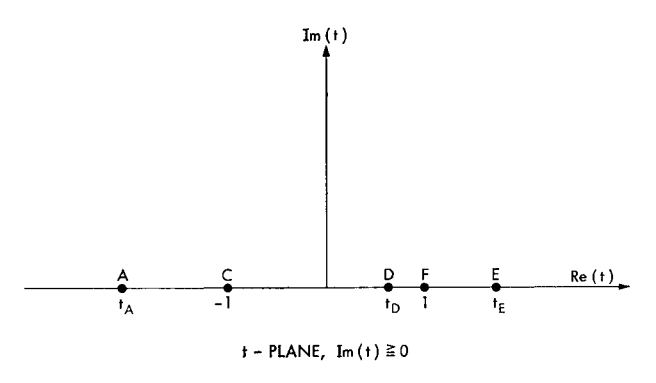


Figure 5 Auxiliary complex plane (see text).

while Newman's depend only on the angle. An attempt to give experimental confirmation of this model was performed by R. E. Norwood, and this is mentioned in Section 4.

2. Analysis

In Fig. 4a, the main jet flow is bounded by AC and ADC, the re-entrant jet by AEF and ADF. At the stagnation point D the flow splits along DC and forms the streamline DF, which is assumed to remain at angle β . This direction is chosen for the re-entrant jet since it seems most plausible that the main orientation of a secondary flow back along the wall would be in the direction of that wall. The offset distance of the downstream wall, d, is measured positive as shown. The flow quantities are normalized in such a manner that the constant pressure region, bounded by EF, is at a pressure which gives a velocity magnitude along EF equal to unity. The main jet flow has velocity magnitude $\alpha < 1$ at A far upstream and all along the free boundary AC.

The curves AC and EF are not known, nor is the point D. Also, the partition of the mass flow from, say, a quantity normalized to unity at A into the quantities δ_F and δ_C at F and C must be determined. The control port width is not a parameter in this model since we do not specify a mass flow into this region but only a pressure along the free streamline boundary of the re-entering jet. Thus the region over which this pressure is exerted is computed in obtaining the free streamline and cannot be prescribed a priori.

It is useful to introduce in the x, y coordinate system with origin at E, the designation of a measurement, s, along the line FDC, as shown in Fig. 4. The equation of the line FDC is then given as

$$z = (s + id)e^{i\beta} \qquad -\infty < s < +\infty. \tag{3}$$

In the complex potential plane w there is a cut beginning at D and extending on one side to F and on the other to C. In the Ω -plane A is the point $(-\ln \alpha, 0)$, D is at ∞ , and F is at $(0, i(\pi + \beta))$.

The mapping from the Ω - to the *t*-plane (Fig. 5) is given by

$$\frac{d\Omega}{dt} = \frac{M\sqrt{t+1}}{(t-t_D)\sqrt{(t-t_A)(t-1)(t-t_E)}}$$

$$t_E > 1 > t_D > -1 > t_A, \quad (4)$$

where the labeled values of t lie along the real t-axis as shown. The value M is a real constant. It may be determined by imposing the condition that at D there is a jump of $i\pi$ in the Ω -plane. Calculating along a semi-circular arc of radius ϵ around D,

$$i\pi = \lim_{\epsilon \to 0} \int_{\epsilon} \frac{d\Omega}{dt} dt = -i(-\pi) \operatorname{Res} \left\{ \frac{d\Omega}{dt}, t = t_D \right\}$$

one obtains

$$M = \frac{\sqrt{(t_D - t_A)(1 - t_D)(t_E - t_D)}}{\sqrt{1 + t_D}}.$$
 (5)

The next steps are to ascertain the behavior of $d\Omega/dt$ along each interval on the real t-axis and to use this in-

formation when the following conditions are imposed:

(a)
$$\Omega_A - \Omega_E = -\ln \alpha$$

(b)
$$\Omega_C - \Omega_A = i\beta$$

(c)
$$\Omega_E - \Omega_F = -i(\pi + \beta)$$
. (6)

The behavior of $d\Omega/dt$ is indicated in the Appendix. The jumps in Ω on the left-hand sides of (a), (b), and (c) are obtained by integrating $d\Omega/dt$ over the appropriate intervals in t.

With some manipulation one obtains

$$\beta = \int_{t_A}^{-1} \frac{M\sqrt{-1 - t} dt}{(t_D - t)\sqrt{(t - t_A)(1 - t)(t_E - t)}}, \text{ or}$$

$$= -\pi + \int_{1}^{t_E} \frac{M\sqrt{1 + t} dt}{(t - t_D)\sqrt{(t - t_A)(t - 1)(t_E - t)}}$$

$$-\ln \alpha = \int_{t_E}^{\infty} \frac{M\sqrt{1 + t} dt}{(t - t_D)\sqrt{(t - t_A)(t - 1)(t - t_E)}}$$
(7)

The mapping from the w-plane to the t-plane is simpler and is most conveniently expressed in the Schwarz-Christoffel form

 $+ \int_{-\infty}^{t_E} \frac{M\sqrt{-1-t} dt}{(t_D-t)\sqrt{(t_A-t)(1-t)(t_B-t)}}.$

$$\frac{dw}{dt} = N \frac{(t - t_D)}{(t - 1)(t + 1)(t - t_A)}$$
(9)

so that $dz/dt = \exp(\Omega) \ dw/dt$. The constant N is chosen in such a way that the upstream width is unity. Since there are simple poles at $t = \pm 1$, and t_A for dz/dt, following the same procedure as in the determination of M in Eq. (5), one obtains

$$N = -\frac{\alpha(1 - t_A)(-1 - t_A)}{\pi(t_D - t_A)}, \qquad (10)$$

and

$$\delta_C = \frac{(1 - t_A)(1 + t_D)}{2(t_D - t_A)} \tag{11}$$

$$\delta_F = \alpha \, \frac{(1 - t_D)(-1 - t_A)}{2(t_D - t_A)} \tag{12}$$

for the widths of the main jet at infinity downstream and of the re-entrant jet at infinity. It is to be observed that the conservation of mass requires that

$$\alpha \cdot 1 = \alpha \delta_C + \delta_F \tag{13}$$

and that it can be shown that (11) and (12) satisfy this

requirement. Therefore, dz/dt may be written in the form

$$\frac{dz}{dt} = \frac{\alpha}{\pi} \left\{ \frac{1}{t-t} - \frac{\delta_C}{t+1} - \frac{1-\delta_C}{t-1} \right\} e^{\Omega(t)}. \tag{14}$$

Equation (14) may now be integrated. One must take care to give the proper expression for the function $\Omega(t)$ in each interval of the t-axis. These are noted in the Appendix. The function z(t) may be obtained and evaluated along boundaries such as EF, DF, et cetera. Setting $t = t_D$ in the expression for z, one obtains $z_D = (s_D + id)e^{i\beta}$ and

$$\frac{\pi}{\alpha} \left[s_D + i(d - \delta_F) \right]$$

$$= C.P. \left\{ \int_{t_D}^1 \left[\frac{1}{t - t_A} + \frac{1 - \delta_C}{1 - t} \right] - \frac{\delta_C}{t + 1} \right] \exp \left[p_1(t) \right] dt$$

$$+ \int_1^{t_E} \left[\frac{1}{t - t_A} - \frac{1 - \delta_C}{t - 1} \right]$$

$$- \frac{\delta_C}{t + 1} \left[\cos p_2(t) - i \sin p_2(t) \right] dt \right\}, \quad (15)$$

where C.P. indicates Cauchy Principal Part when $t \to 1$. The values $p_1(t)$ and $p_2(t)$ are real elliptic integrals defined as

$$p_{1}(t) = \int_{t}^{1} \frac{1}{t - t_{D}} \left[\frac{t_{E} - t_{D}}{t_{E} - t} \frac{1 - t_{D}}{1 - t} \right] dt,$$

$$\frac{t_{D} - t_{A}}{t - t_{A}} \frac{1 + t}{1 + t_{D}} \right]^{1/2} dt,$$

$$t_{D} < t \le 1, \quad p_{1}(t) \ge 0 \quad (16)$$

$$p_{2}(t) = \int_{1}^{t} \frac{1}{t - t_{D}} \left[\frac{t_{E} - t_{D}}{t_{E} - t} \frac{1 - t_{D}}{t - 1} \right] dt$$

$$\frac{t_{D} - t_{A}}{t - t_{A}} \frac{1 + t}{1 + t_{D}} dt$$

$$1 \le t \le t_{E}, \quad 0 \le p_{2}(t) \le \pi + \beta. \quad (17)$$

In a formal manner Eqs. (7), (8), (11), (12), and (15) are the results. There are six quantities s_D , d, δ_C , δ_F , β , and α . Given the flow and the geometry, one has β , α , and d with which to obtain s_D , δ_C , and δ_F . Actually, because of the difficult expressions it is clear that one will have to proceed in an indirect fashion, working from parameters in the t-plane back to the physical, z-plane. This is described in the following section.

3. Numerical analysis

The solution of the problem has been expressed in terms of the three parameters of the mapping, t_A , t_E , and t_D . Now, the angle β and the flow parameters α , δ_C , and δ_F

can be expressed in terms of two other parameters k and ψ_2 which are combinations of t_A , t_E , and t_D :

$$k^{2} = \frac{(t_{E} - 1)(-1 - t_{A})}{(t_{E} + 1)(1 - t_{A})}, \qquad (k'^{2} = 1 - k^{2}) \quad (18)$$

$$\sin^2 \psi_2 = \frac{(t_E + 1)(1 - t_D)}{2(t_E - t_D)}.$$
 (19)

For given values of k and ψ_2 , one can compute β and α :

$$\frac{\beta}{2} = \sin \psi_2 (1 + k^2 \tan^2 \psi_2)^{1/2} K - EF(\psi_2, k') - KE(\psi_2, k') + KF(\psi_2, k')$$

$$\ln (\alpha^{-1/2}) = \sin \psi_2 (1 + k^2 \tan^2 \psi_2)^{1/2} K'$$
(20)

$$-K'E(\psi_2,k')+E'F(\psi_2,k')$$

$$\delta_C = (1 + k^2 \tan^2 \psi_2)^{-1} \tag{22}$$

$$\delta_F = \alpha (1 - \delta_C), \tag{23}$$

where K, E and K', E' are the complete elliptic integrals of moduli k and k' respectively, and $F(\psi_2, k')$ and $E(\psi_2, k')$ are the incomplete elliptic integrals of argument ψ_2 , and modulus k'. These computations were accomplished by employing existing library subroutines in the FORTRAN program. It was found, with some experimental computations, that for values of α and β of interest in connection with the jet amplifier, k is close to unity and ψ_2 is small. It can be shown that for a fixed $\beta < \pi/4$ and k > 0.8.

$$\sin \psi_2 \cong \frac{\beta}{2(K-E)}. \tag{24}$$

Based on this relation an iteration scheme was employed to compute an exact value of ψ_2 , and hence α , δ_C , and δ_F for a given k and a fixed β .

The offset distance d and the stagnation point s_D could then be computed according to the following formulas:

$$\frac{\pi}{\alpha} \left[d - \delta_F \right] = \int_1^{t_E} \left[\frac{1 - \delta_C}{t - 1} + \frac{\delta_C}{t + 1} \right]$$

$$- \frac{1}{t - t_A} \sin \left[p_2(t) \right] dt, \qquad (25)$$

$$\frac{\pi}{\alpha} s_D = \text{C.P.} \left\{ \int_{t_D}^1 \left[\frac{1}{t - t_A} + \frac{1 - \delta_C}{1 - t} \right] \right.$$

$$- \frac{\delta_C}{t + 1} \exp \left[p_1(t) \right] dt$$

$$+ \int_1^{t_E} \left[\frac{1}{t - t_A} - \frac{1 - \delta_C}{t - 1} \right]$$

$$- \frac{\delta_C}{t + 1} \cos \left[p_2(t) \right] dt \right\}, \qquad (26)$$

where $p_1(t)$ and $p_2(t)$ are given in (16) and (17).

Although $p_1(t)$ and $p_2(t)$ may be integrated explicitly

in terms of elliptic integrals, the integrals needed in evaluating d and s_D cannot be integrated explicitly. The complete expressions in (25) and (26) were therefore integrated numerically. Note that the singularities at $t=t_E$ are integrable for all integrals. It can also be shown that the first integral in evaluating s_D is integrable at $t=t_D$, and the integral in evaluating d is integrable at t=1. The numerical integrations were carried out in the intervals $t_D+\epsilon \le t \le 1-\epsilon$, and $1+\epsilon \le t \le t_E-\epsilon$, with

$$\epsilon \leq \frac{(t_E-1)(1-t_D)}{N(t_E-t_D)},$$

(21)

for some large $N \ge 25$. The contributions of the Cauchy Principal Part and the integrals near the integrable singularities were evaluated by explicitly integrating the expressions using approximate integrands near these singularities. By fixing the relative locations of t_A , t_E , and t_D on the mapping plane for those combinations of k and ψ_2 used in evaluating β and α , the computations of d and s_D could then be carried out accordingly.

A FORTRAN program for the above numerical procedure was written for the case $2 < t_E < \infty$. Numerical results indicate that both d and s_D increase as t_A moves along the real axis on the complex t-plane toward t_E which is, in turn, moved toward t = 1. Thus, t_A may take values such that either $-\infty < t_A < -1$ or $\infty > t_A > t_E > 2$. If one desires the solution for a fixed d, one would have to find the exact relative location of t_A , t_E , and t_D which would include the possibility that t_E may be located such that $-\infty < t_E < t_A < -1$. This would require a new set of formulas to compute d and s_D . It was therefore felt that extremely small variations in d were tolerable in view of the far more extensive calculations that would be required if d were held fixed. The plots showing s_D vs α have, therefore, a slightly different value of d at each plotted point, as indicated in Fig. 6. The actual values of d which were computed give d > 0 for small α and d < 0for large α . An idea of the small size of d can be obtained from Fig. 6. Since both d and s_D increase as t_E moves toward t = 1, the results of the computed $d \neq 0$ would mean that the computed s_D 's, interpreted as d = 0, are underestimated for large α and overestimated for small α . If d < 0, this would also mean that a gap of at least $d / \csc \beta$ has to be provided between the corner E and the beginning of the wall in the physical plane, as is evidenced in Fig. 7.

4. Discussion of results

The main result of the work is shown in Figs. 8 and 9 where the variation of s_D with α and β is indicated. For fixed α , s_D varies linearly with β . The actual values of s_D (recall that it is normalized with respect to the upstream jet width) are quite small compared to those obtained by

Newman.⁷ R. E. Norwood of the IBM General Products Development Laboratory has made a single experiment with the control port completely closed off. For $\beta=20^{\circ}$ and $\alpha\cong0.7$, Norwood could only obtain a single constant pressure reading to identify the separation region with his experimental setup. This, however, indicated s_D was somewhere between 0.5 and 1.0, which gives some encouragement. It may be possible to rearrange the equipment so as to carry out further experiments.

Figures 10 and 11 show the variation of δ_C and δ_F with α for two values of β . Note the small percentages of fluid lost into the re-entrant jet.

Although the shortcomings of the model are obvious, the results seem to fall into line with what could be expected from extending the analysis of Newman to small values of β . Norwood's single experiment is also encouraging. One could pursue the idea that the momentum calculated here as disappearing onto a second Riemann sheet is related to the momentum entrained by a turbulent free jet or wall jet. What is discouraging is the difficulty

of moving upward in the hierarchy of problems described in the Introduction because of the hard numerical calculations. These are to be expected in any model wherein the boundary conditions are mixed in terms of velocities or pressures and flow direction. Perhaps a linearized free streamline model, in the manner employed by Tulin¹² in cavitation problems, would lessen the calculational difficulty.

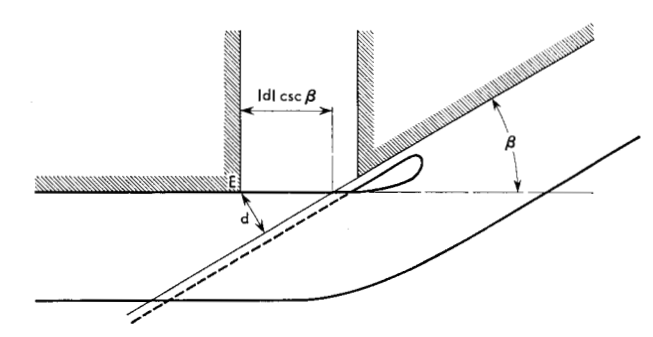


Figure 7 Minimum control port width when d < 0.

Figure 6 Plot of d, offset of wall, vs α , ratio between uniform jet velocity far upstream and that along free boundary of re-entrant jet, for $\beta=11.5^\circ$ and $\beta=18^\circ$.

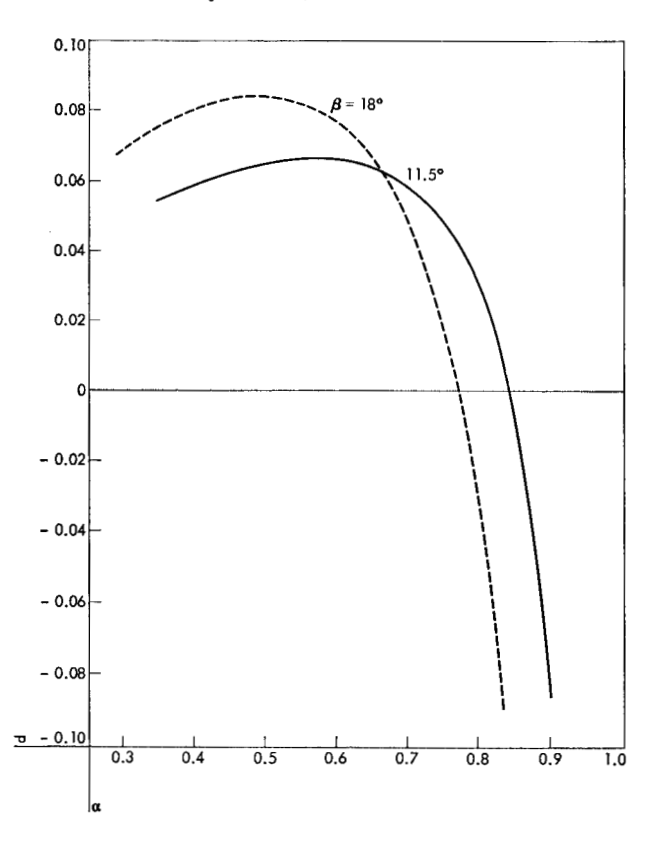
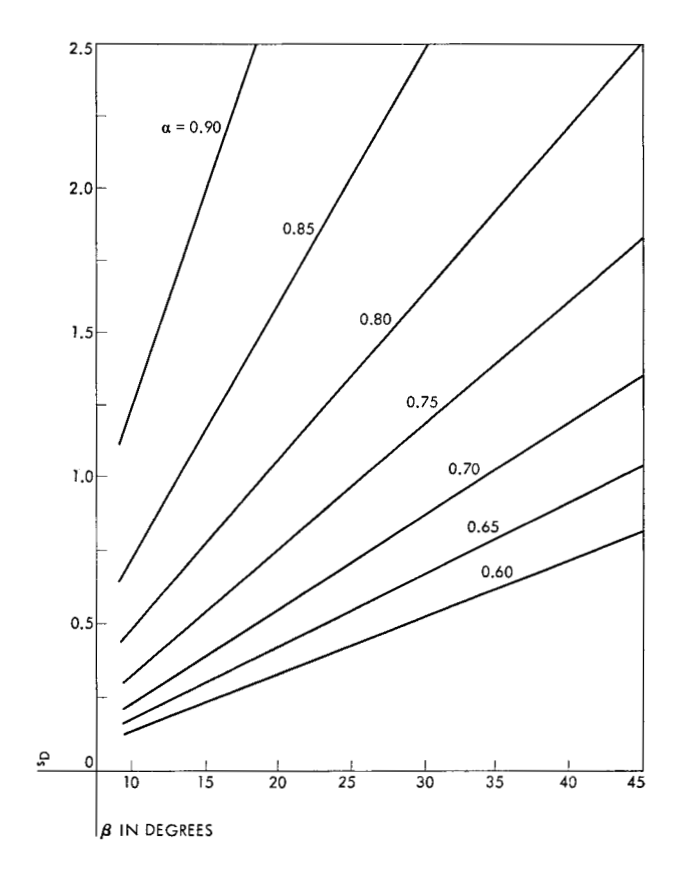
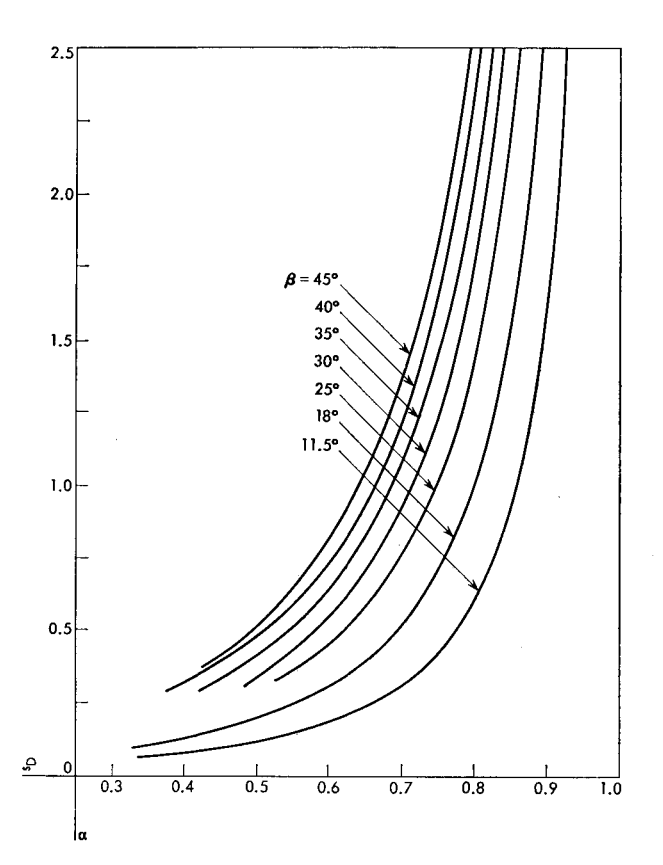


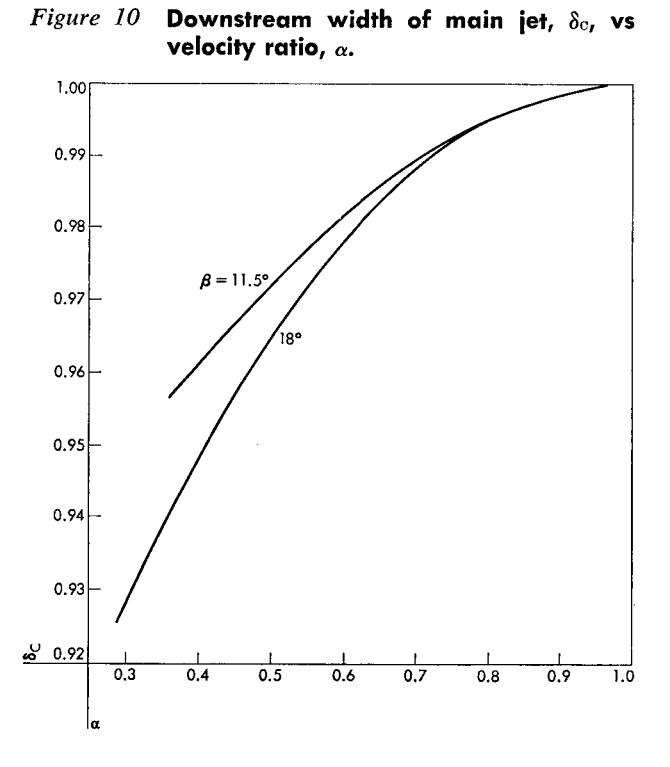
Figure 8 Location of stagnation point, s_b , vs angle of wall and axis of channel, β .





Location of stagnation point, $s_{\scriptscriptstyle D}$, vs ve-Figure 9 locity ratio, α .

Figure 10



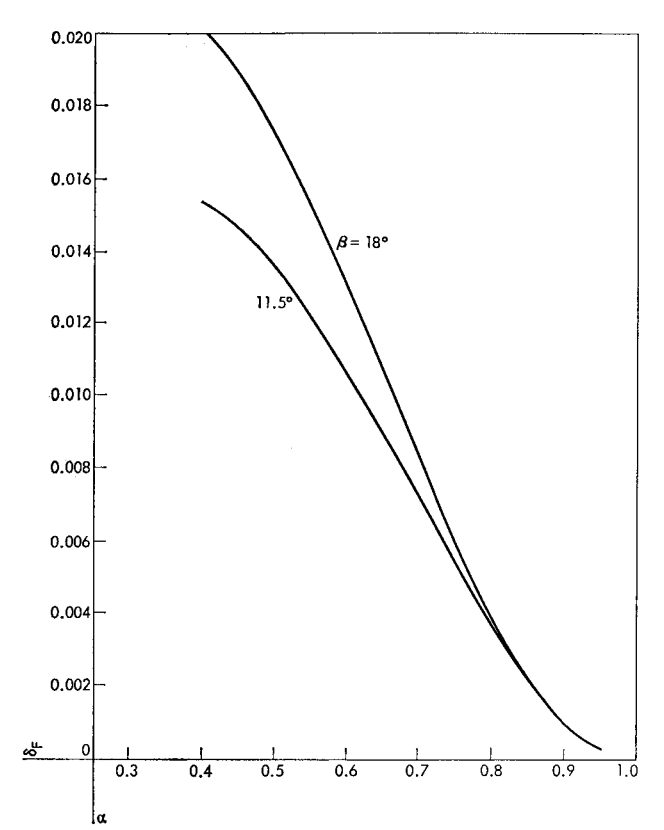


Figure 11 Downstream width of re-entrant jet, $\delta_{\rm F}$, vs velocity ratio, α .

Appendix

1. The behavior of $d\Omega/dt$ along the real t-axis:

$$\frac{d\Omega}{dt} = \frac{M\sqrt{t+1}}{(t-t_D)\sqrt{(t-t_A)(t-1)(t-t_E)}}, \quad t > t_E$$

(purely real and positive)

$$= -i \frac{M\sqrt{t+1}}{(t-t_D)\sqrt{(t-t_A)(t-1)(t_E-t)}},$$

$$1 < t < t_E$$

(purely imaginary and negative)

$$= -\frac{M\sqrt{1+t}}{(t-t_D)\sqrt{(t-t_A)(1-t)(t_E-t)}},$$

$$-1 < t < 1$$

(purely real, positive when $t < t_D$, negative when $t > t_D$)

$$\frac{d\Omega}{dt} = i \frac{M\sqrt{-1 - t}}{(t_D - t)\sqrt{(t - t_A)(1 - t)(t_E - t)}},$$

$$t_A < t < -1$$

(purely imaginary, and positive)

$$= \frac{M\sqrt{-1-t}}{(t_D-t)\sqrt{(t_A-t)(1-t)(t_E-t)}}, \quad t < t_A$$

(purely real and positive).

 $d\Omega/dt$ has a simple pole at t_D and is regular elsewhere.

2. The proper form of the integrals for $\Omega(t)$ in the various intervals along the *t*-axis is given here.* The numbers at the right refer to numbered integrals in Byrd and Friedman.¹³ All integrals are real.

Acknowledgments

The authors would like to express appreciation for the programming assistance given by Arthur Priver of Brown University, who spent the summer of 1962 at the Thomas J. Watson Research Center. They would also like to thank R. E. Norwood, IBM General Products Development Laboratory, Endicott, for discussing this problem with them and for carrying out the experiment.

References

 Anonymous, Control Engineering 7, 5 (May 1960). Also, for a report on a similar Russian device, see R. N. Auger, Automatic Control 11, 43 (December 1960).

- R. E. Norwood, paper presented at the ASME Winter Annual Meeting, Nov. 25-30, 1962, New York, and published in *Fluid Jet Control Devices*, ASME, New York, a collection of the papers presented on this topic at a symposium at that meeting. The collection contains other papers of general interest.
- R. A. Comparin, H. H. Glättli, A. E. Mitchell, H. R. Muller, published in *Fluid Jet Control Devices*, as above.
- See also the papers presented at the Fluid Amplification Symposium, Diamond Ordnance Fuze Laboratory, National Bureau of Standards, Washington, D. C., Oct. 2-4, 1962.
- For a description of Coanda's ideas, see A. Metral, Proc. Fifth Int. Cong. Appl. Mech., p. 256 (1938).
- C. Bourque and B. G. Newman, Aero. Quarterly XI, 201 (1959).
- B. E. Newman, Boundary Layer and Flow Control, I edited by G. V. Lachmann, Pergamon Press, 1961, pp. 232-264.
- 8. R. A Sawyer, J. Fluid Mech. 9, 543 (1960). I. Greber, in Fluid Jet Control Devices, see Reference 2.
- D. A. Efros, Doklady Akad. Nauk, U. S. S. R., 51, 267 (1946) and 60, 29 (1948).
- 10. G. Kreisel, Adm. Res. Lab. Rep. R1/H/36 (1946). For this reference and for additional information on this model, see G. Birkhoff and E. H. Zarantonello, Jets, Wakes, and Cavities, Academic Press, New York, 1957, pp. 56 and 146; also M. I. Gurevich, Theory of Jets and Wakes in an Ideal Fluid (in Russian), Moscow, 1961.
- 11. A. D. Cox and W. A. Clayden, J. Fluid Mech. 3, 6 (1958).
- 12. M. P. Tulin, David Taylor Model Basin Report No. 834, 1953.
- P. F. Byrd and M. D. Friedman, Handbook of Elliptic Integrals for Engineers and Physicists, Springer-Verlag, Berlin, 1954.

Received December 6, 1962

* Form of the integrals for Ωt

$$t_E < t: \qquad \Omega(t) = M \int_{t_E}^{t} \frac{-1 - t}{(t_D - t)\sqrt{(t - t_E)(t - 1)(t + 1)(t - t_A)}} dt \qquad (258.40)$$

$$t < t_A: \qquad (-\ln \alpha) - \Omega(t) = M \int_t^{t_A} \frac{-1 - t}{(t_D - t)\sqrt{(t_E - t)(1 - t)(-1 - t)(t_A - t)}} dt$$
 (251.40)

 $t_A \leq t < -1$:

$$(-\ln \alpha) + i\beta - \Omega(t) = iM \int_{t}^{-1} \frac{-1 - t}{(t_D - t)\sqrt{(t_E - t)(1 - t)(-1 - t)(t - t_A)}} dt$$
 (253.40)

 $-1 < t < t_D$:

$$\Omega(t) - (-\ln \alpha) - i\beta = M \int_{-1}^{t} \frac{1+t}{(t_D - t)\sqrt{(t_E - t)(1-t)(t+1)(t-t_A)}} dt$$
 (254.40)

$$t_D < t < 1: \ i(\pi + \beta) - \Omega(t) = M \int_t^1 \frac{1+t}{(t_D - t)\sqrt{(t_E - t)(1-t)(t+1)(t-t_A)}} dt$$
 (255.40)

$$1 \le t < t_E: -\Omega(t) = iM \int_t^{t_E} \frac{1+t}{(t_D-t)\sqrt{(t_E-t)(t-1)(t+1)(t-t_A)}} dt.$$
 (257.40)